CO Desorption Rate Dependence on CO Partial Pressure over Platinum Fuel Cell Catalysts

J. C. Davies[1], R. M. Nielsen[1], L. B. Thomsen[1], I. Chorkendorff[1]*, Á. Logadóttir[2], Z. Lodziana[2], J. K. Nørskov[2], W. X. Li[3], B. Hammer[3], S. R. Longwitz[4], J. Schnadt[4], E. K. Vestergaard[4], R. T. Vang[4] and F. Besenbacher[4]

[1] Interdisciplinary Center for Catalysis (ICAT), Department of Physics, Department of Chemical Engineering, Technical University of Denmark, Building 312, DK-2800 Lyngby, Denmark

[2] Center for Atomic-Scale Materials Physics (CAMP), Department of Physics, Technical University of Denmark, Building 307, DK-2800 Lyngby, Denmark

[3] Interdisciplinary Nanoscience Center and Institute of Physics and Astronomy, University of Aarhus, Ny Munkegade, DK-8000 Aarhus C, Denmark

[4] Center for Atomic-Scale Materials Physics (CAMP), Interdisciplinary Nanoscience Center, and Department of Physics and Astronomy, University of Aarhus, DK-8000 Aarhus C, Denmark

Abstract

Carbon monoxide adsorption on high area platinum fuel cell catalysts was investigated. Isotopic exchange experiments were performed to determine the exchange rate (k) of CO under different partial pressures of CO (p_{CO}) in argon. A linear dependence of $\ln(k)$ with $\ln(p_{CO})$ was observed. This pressure dependence of the rate of exchange is explained by considering a change in surface coverage of CO with different CO pressures and a subsequent reduction in the CO binding energy as demonstrated by Density Functional Theory (DFT) calculations. High Pressure Scanning Tunneling Microscopy (HP STM) studies on the Pt(111) surface have also displayed a pressure dependency of the coverage consistent with this data. The relevance of these observations to the Polymer Electrolyte Membrane Fuel Cell (PEMFC) anode reaction is discussed.

Keywords: Co-Tolerance, Ligand Effect, PEM Fuel Cell, Platinum, Ruthenium

1 Introduction

Proton Exchange Membrane Fuel Cells (PEMFC) are the most likely fuel cells to achieve commercialisation for automotive purposes due to their low operating temperatures and their inherent properties of being lightweight, producing high current densities and containing no corrosive materials [1]. At the anode of the fuel cell hydrogen dissociation and oxidation to protons occurs. This electrode is generally platinum-based due to the high current densities obtained [2, 3] and its inherent stability within fuel cell operating conditions. The protons formed then pass through a proton conducting membrane to the supported platinum cathode where they combine with oxygen to form water. If the hydrogen feed to the anode is to be produced at reasonable prices, inline reformation of a hydrocarbon species, e.g., methanol, is a viable option. Reforming methanol by partial oxidation or steam reforming produces a hydrogen feed which can contain approximately 1% CO, along with 25% CO_2. It is very difficult to remove this CO entirely and as little as 20 ppm of CO is known to poison the hydrogen oxidation reaction at the anode by binding strongly to the platinum surface [4]. It has been shown that by alloying platinum with ruthenium the anode tolerance to CO can be increased [5]. Currently, there are two proposed mechanisms for this promotion:

i) The bifunctional effect [6, 7]: It can be demonstrated that alloying Pt and Ru (with an optimal ratio of 50:50)

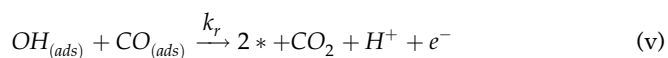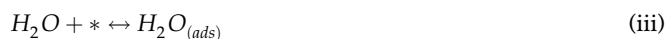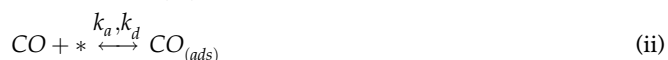[*] *Corresponding author, ib.chorkendorff@fysik.dtu.dk*

reduces the overpotential required for the oxidation of pure CO to CO_2 by water [8–12]. This reduction in overpotential is due to the more facile dissociation of water on ruthenium. This mechanism has been further elucidated on model alloy systems prepared in vacuum and then investigated electrochemically [13–15] and also theoretically [16–18].

ii) The ligand effect [1, 19–21]: Here, alloying ruthenium with platinum alters the chemical properties of the surface platinum atoms. It has been found both experimentally [14, 22] and theoretically [16–18, 23–26] that the Pt-CO bond strength in a platinum/ruthenium alloy is significantly reduced compared to that on pure platinum.

In the situation where CO oxidation occurs in the presence of hydrogen, it has been suggested that there may be a combined mechanism where both of the above processes are relevant [6, 27].

An important question in connection with the unravelling of the two possible mechanisms is whether CO from the reactant stream is in equilibrium with CO on the surface. If this is the case, then the ligand effect must be a factor, a weaker CO bond must lead to a lower CO coverage. This of course does not preclude a contribution from the bifunctional effect.

This can be expressed using the following kinetic description of the processes occurring at a fuel cell anode:

$$H_2 + 2* \leftrightarrow 2H_{(ads)} \tag{i}$$

$$CO + * \overset{k_a, k_d}{\longleftrightarrow} CO_{(ads)} \tag{ii}$$

$$H_2O + * \leftrightarrow H_2O_{(ads)} \tag{iii}$$

$$H_2O_{(ads)} \rightarrow OH_{(ads)} + H^+ + e^- \tag{iv}$$

$$OH_{(ads)} + CO_{(ads)} \overset{k_r}{\longrightarrow} 2* + CO_2 + H^+ + e^- \tag{v}$$

$$H_{(ads)} \rightarrow * + H^+ + e^- \tag{vi}$$

It can be seen that steps (ii) and (v) are the only two involving CO. At steady state the coverage of CO will be governed by the following equation:

$$\frac{d\theta_{CO}}{dt} = k_a p_{CO}(1 - \theta_{CO}) - k_d \theta_{CO} - k_r \theta_{CO} = 0$$

or

$$\theta_{CO} = \frac{k_a p_{CO}}{k_a p_{CO} + k_d + k_r} = \frac{k_a p_{CO}}{k_a p_{CO} + k_d} \times \left(\frac{1}{1 + \frac{k_r}{k_a p_{CO} + k_d}} \right) \tag{1}$$

Rearranging this equation, it can be shown that the steady state coverage of CO on the surface can be expressed as two terms, the first of which is the coverage determined by the CO adsorption equilibrium, whilst the second term is a correction due to the effect of CO oxidation. From this second term it can be determined that for the rate of oxidation of CO

to play a significant role it would have to be large compared to the combined rates of adsorption and desorption.

It is with this in mind that the equilibrium rates of desorption will be determined during the course of this paper.

The adsorption of CO on platinum is a thoroughly researched area, but the majority of surface studies are limited to the high vacuum regime. In nanoscale platinum particles the (111) face is favoured at the surface, hence this system will be treated in detail here. Ertl et al. have studied the adsorption of CO at 170 K on Pt(111) by LEED and TPD [28]. A diffuse ($\sqrt{3}$ x $\sqrt{3}$)R30° LEED pattern was observed for an overlayer of $\theta \leq 0.33$ and spectroscopic evidence from EELS [29, 30] and RAIRS [31] experiments have shown that, at this coverage, only linear CO is present (~2110 cm^{-1}). At a coverage of $\theta \leq 0.5$ this transforms into a c(4 × 2) overlayer with both linear and bridge-bound species present in a 1:1 ratio [31]. The presence of a c(4 × 2) structure below $\theta = 0.5$ is explained by island formation of the adsorbed species. Further splitting of the c(4 × 2) structure is observed up to a saturation coverage of 0.67.

Recently, work has been performed by several groups in an attempt to bridge the pressure gap in this regime. Besenbacher et al. have observed CO overlayers on Pt(111) in the high pressure regime by STM [32]. A maximum coverage of 0.68 ML was again obtained leading to the conclusion that raising the pressure was equivalent to lowering the temperature, as long as the thermodynamic equilibrium structure remains kinetically accessible. Sum Frequency Generation studies by Rupprechter et al. observed a 40% increase in the intensity of the linear bound CO from the c(4 × 2) structure to the saturation coverage. The coverage dependence on the binding energy of the CO on Pt(111) is well known under these pressure regimes. Ertl et al. observed an initial adsorption energy of 138 kJ mol^{-1} at room temperature, reducing to 62 kJ mol^{-1} at the saturation coverage of 0.67 [28]. Microcalorimetry experiments by Yeo et al. have also demonstrated a shift in the heat of adsorption from a value of 183 kJ mol^{-1} at a coverage of 0.05 ML down to a value of 75 kJ mol^{-1} at a coverage of 0.75 ML [33].

In previous studies, which were concerned with investigating the replacement of C^{13}O preadsorbed by gaseous C^{12}O on polycrystalline platinum [34] no effect of changing pressure was observed, but these experiments were performed in a low pressure regime (1.5–4.6 × 10^{-7} mbar). However, a dependence on temperature was observed. A value of 90 kJ mol^{-1} for the activation energy was obtained leading to a rate of desorption of 3.50 × 10^{-9} mol m^{-2} s^{-1}.

An isothermal kinetic study of hydrogen induced CO displacement has previously been performed by Parker et al. [35]. They observed that chemisorbed CO could be completely removed from the Pt(111) surface at temperatures from 318–348 K and hydrogen pressures above 2.6 × 10^{-2} mbar. In this temperature range only a fraction of the CO is removed by thermal desorption. They proposed that repulsive interactions between the CO and atomic hydrogen lead to lower values of the desorption activation energy.

It will be demonstrated, by isotopic exchange experiments and DFT calculations, that there is a significant relationship between the pressure of CO above a platinum catalyst surface and the subsequent desorption rate, binding energy and coverage of the CO. These observations will be used to elucidate the mechanism for fuel cell anode catalysis.

2 Experimental

Experiments were performed on the system given in Figure 1. The sample used was a commercial membrane electrode assembly or MEA (Electrochem. Inc.) consisting of a Nafion® 115 membrane, both sides of which were mounted with Toray carbon paper impregnated with the highly dispersed platinum catalyst. The catalyst loading was 1 mg cm^{-2} and the total area of each carbon electrode 5 cm^2. The electrode was mounted in a stainless steel cell between brass connecting flow field plates.

For the purposes of the experiments presented, the system was used in a flow mode and only one electrode was used for adsorption experiments, i.e., open circuit mode with pure argon flow on the cathode side. The gas content was investigated using a quartz tube sniffer connected to a mass spectrometer [36]. The gas dosing system allowed for fast interchange between a variety of different gases. The highest available gas purities were always used. All experiments were performed at room temperature and no humidification was used in the gas streams.

Measurements were also performed on a Pt(111) single crystal using a combination of a UHV STM and a high pressure STM with the facility for *in situ* scanning over a range of 13 orders of magnitude of pressure from 10^{-10} mbar up to 1 bar. The system used for these studies is described in detail elsewhere [37].

3 Calculations

To calculate adsorption energies Density Functional Theory (DFT) calculations were used. The DFT calculations were based on a plane-wave expansion of the wave functions, a RBPE description of exchange and correlation effects [38], and ultra-soft pseudopotentials [39]. Plane waves with kinetic energies of up to 25 Ry were used. The self-consistent electron density was determined by iterative diagonalization of the Kohn-Sham Hamiltonian, Fermi-population of the Kohn-Sham states ($k_B T = 0.1$ eV), and Pulay mixing of the resulting electronic density [40]. All total energies have been extrapolated to $k_B T = 0$ eV. The Pt(111) surface was studied and was modelled with 4 layer slabs and with 6 layers of vacuum between the slabs. A fcc structure with a lattice constant of $a = 4.02$ Å was used. The CO and the top-most Pt layer were allowed to relax.

The aim of the study was to find the adsorption energy of CO at different coverages. To obtain these differences in coverage the adsorption energy was calculated using several different surface unit cells, (1×1) ($\theta = 1.0$), (2×2) ($\theta = 0.25$), $(\sqrt{3} \times \sqrt{3})$R30° ($\theta = 0.33$), c($4 \times 2$) ($\theta = 0.5$) and a unit cell containing 13 CO molecules ($\theta = 0.68$) as is shown in Ref. [32]. The k points used in the calculations for the Pt(111) surface are a regular grid of $4 \times 4 \times 1$ and $6 \times 6 \times 1$ for the coverages $\theta = 0.25$, 0.333. For $\theta = 0.5$ and 1.0, 4 and 54 special k points were used. One special k point was used to find the CO adsorption energy at $\theta = 0.68$.

CO on Pt(111)

The rich experimental evidence of the adsorption properties of CO on Pt(111) are summarised in Figure 2 together with the calculated integral heats of adsorption, E_{ads}^{int}. A strong coverage dependence of E_{ads}^{int} is evident irrespective of the experimental method used. Theoretical predictions give a slightly larger coverage dependence.
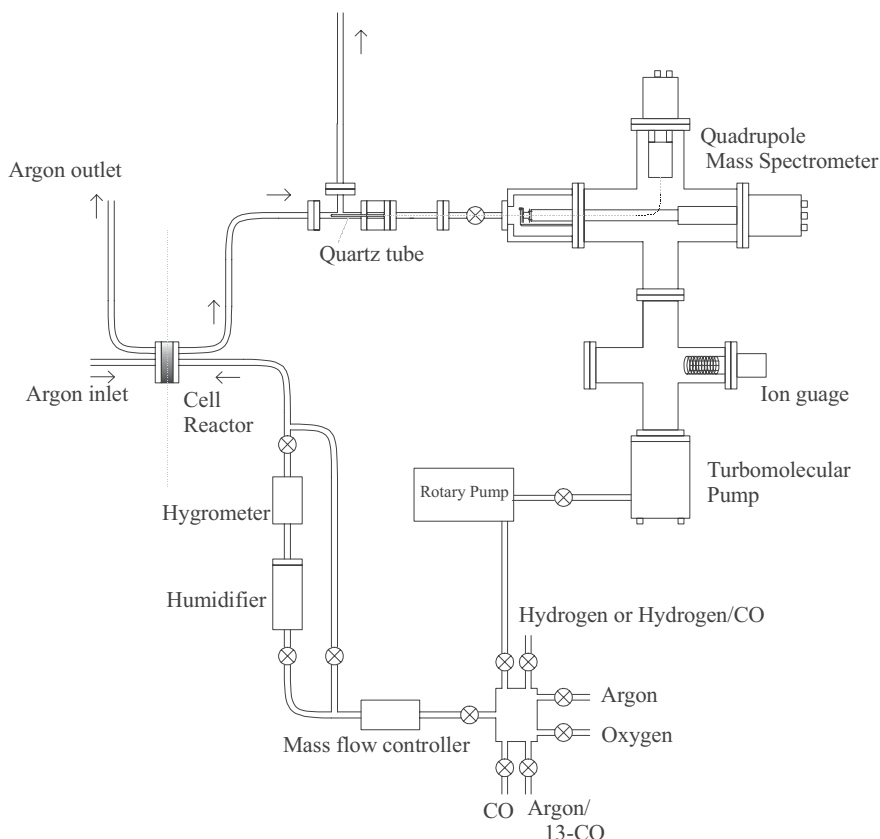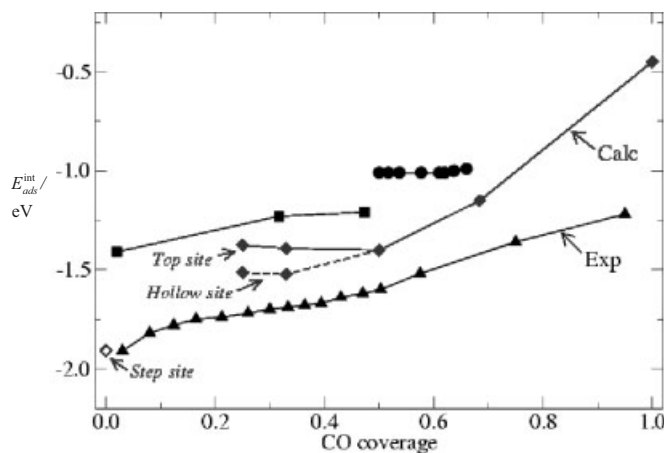

Fig. 1 Apparatus used for flow data measurement.

Fig. 2 The integrated enthalpies for CO adsorption (E_{ads}^{int}) at different coverages. The DFT results (diamonds) are compared to three different sets of experimental results (triangles, circles and squares) taken from [33], where differential enthalpies have been changed to integrated enthalpies for comparison with the calculated results. The enthalpy for CO adsorbed at a step site (open diamond) is taken from [41].

4 Results and Discussion

Initially, the Pt catalyst used was characterised experimentally by adsorption with CO, and subsequent oxidation with O_2. CO was dosed on the high area catalyst surface by exposure of the surface to a flow of CO at 1 bar pressure for approximately 15 min. (hereby ensuring saturation coverage). The flow of CO was then replaced by an argon flow for a time of 20 min. to remove background CO, and was subsequently titrated with O_2. The m/z 44 profile was measured during oxygen exposure and a CO_2 production profile could also be measured in the mass spectrometer (Figure 3). From this it was necessary to subtract a background arising from
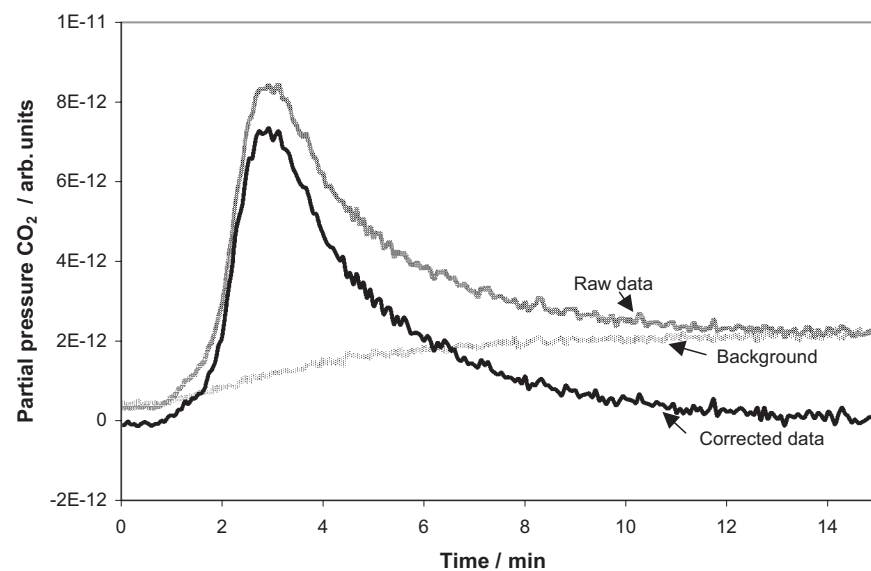
CO_2 formed by oxygen reaction within the mass spectrometer. This background was measured by switching from pure argon to O_2 over a catalyst previously oxygen passivated. In this manner no response is expected from the catalyst and the signal observed is solely due to an increased background of CO_2 in the mass spectrometer, due to the increased pressure of oxygen. From the area of the corrected peak the number of moles of CO_2 can be determined, and then, making certain assumptions, an overall surface area for the catalyst can be approximated. If it is assumed that the saturation coverage is 0.68, as observed on Pt(111), then a surface area of 0.58 m^2 is obtained. Assuming that the particles are spherical then an average particle size of ~2.5 nm is obtained. It should be noted that 0.68 is the coverage calculated on Pt(111) at 1 bar CO pressure, and that, as shall be demonstrated within the course of this article, the coverage after exposure to 1 bar pressure of Ar for a period of 20 min. will be lower than this value. However, as a direct value cannot be measured, 0.68 was determined to be accurate enough for the purpose of determining the approximate particle size and total surface area.

The next stage was to investigate the stability of overlayers of adsorbed $C^{13}O$ on exposure to flows of certain gases and gas mixtures in order to determine the exchange rate for CO from small platinum particles under these conditions.

Firstly, an overlayer of adsorbed CO was exposed to a flow of argon for differing lengths of time and the CO was then titrated with O_2 and the relative coverage obtained (Figure 4). This was in order to determine that there was no effect due to the oxidation of small levels of contaminant species in the pure gases. It can be seen that the coverage decreases to a limiting value after about 4 h, but after this time stabilises and no further reduction is observed. The latter observation is in good agreement with the traditional view of CO poisoning in the PEMFC by a strongly bound overlayer. Note that the depletion in CO coverage is also shown, as observed in the situation where there is oxygen present in the gas stream at a fixed level of contamination. Here, the depletion of CO due to oxidation by contaminant oxygen is strongly observed.

It is not known whether the observation of a decrease in coverage within the first few hours is a real effect or due to the readsorption of some CO from the background (in these experiments where CO is dosed at 1 bar, a slowly decaying background of CO is observed). However, this could tentatively be ascribed to CO in a higher coverage regime at a pressure of 1 bar, slowly desorbing down to its equilibrium level at a pressure of 1 bar of argon, which appears to be attained after a few hours, particularly as the ratio of the highest and lowest cov-

Fig. 3 The evolution of CO_2 arising from the titration of adsorbed CO with 1 bar of O_2. The subtraction of the background obtained due to reaction of oxygen in the mass spectrometer is also shown.
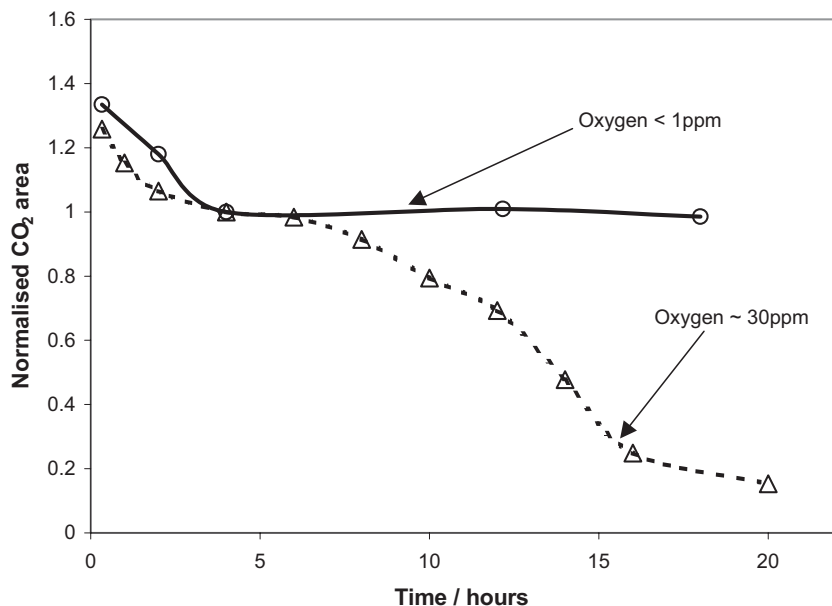
Fig. 4 Plot of normalised CO₂ peak area against time of exposure. CO is dosed at 1 bar, then replaced by a flow of argon. After a given exposure time the remaining CO is titrated with O₂ to produce CO₂. Data is shown for an oxygen-free and oxygen contaminated system.
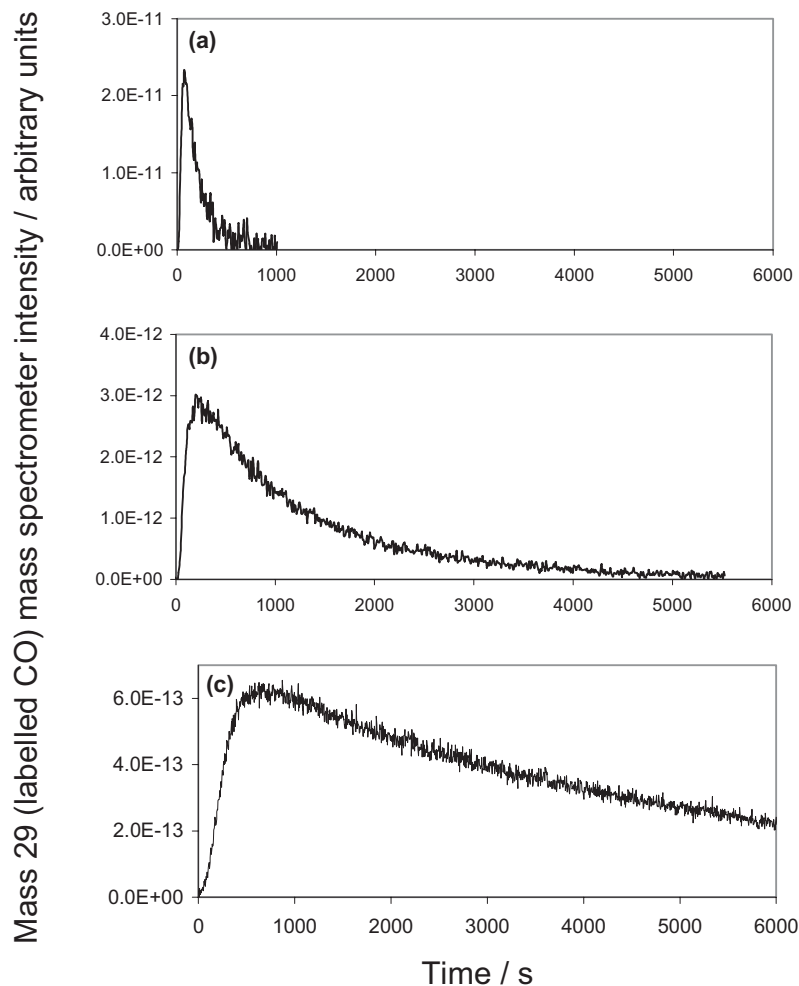

Fig. 5 Plots showing C¹³O desorption in flows of: (a) 1 bar CO, (b) 1000 ppm CO in argon and (c) 100 ppm CO in argon from the platinum electrocatalyst.

erages observed is approximately the same as the ratio between the coverage observed by Besenbacher et al. at 1 bar CO of 0.68 [32] and the coverage observed under vacuum on Pt(111) of 0.5 [32].

Secondly, an overlayer of C¹³O was adsorbed on the platinum surface and a stream of pure C¹²O (1%C¹³O) was passed over the surface at 12 ml min⁻¹. The level of C¹³O in the exit stream was monitored and it was found that the C¹³O was almost entirely removed after 10 min. Reducing the C¹²O content in the stream to 1000 ppm C¹²O in argon lead to a reduction of the rate of removal of C¹³O from the surface. In addition, a similar exchange experiment was performed for 100ppm CO in argon, a concentration which is not unlike that of the fuel cell supply gas [1]. Figure 5 shows the measured traces for desorbing C¹³O in these experiments. Figure 6 shows a plot of ln(θ) versus time including additional data for a C¹²O overlayer exposed to 1% C¹³O, and a C¹³O overlayer exposed to a flow of pure hydrogen. It can be seen that at room temperature virtually no CO desorbs in the time period of 10,000 seconds in pure hydrogen, which seems reasonable, considering that hydrogen interacts more weakly with platinum than CO does. This was confirmed by titrating the remaining C¹³O with oxygen after the period of hydrogen exposure. In contrast Gland et al. have determined that at 318–348 K the presence of hydrogen at a pressure of ~3 mbar strongly influences the desorption of CO on a Pt(111) single crystal [35]. No observable desorption rate is seen under these conditions within the detection limit of the experiments.

The kinetic regime for this system is as follows, where * represents an adsorption site:
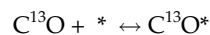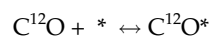
$$C^{12}O + * \leftrightarrow C^{12}O*$$

$$C^{13}O + * \leftrightarrow C^{13}O*$$

From this the following kinetic expressions can be derived:

$$\frac{d\theta_{C12O}}{dt} = k_2^+ P_{C12O}\theta_* - k_2^- \theta_{C12O} \qquad (2)$$

$$\frac{d\theta_{C13O}}{dt} = k_1^+ P_{C13O}\theta_* - k_1^- \theta_{C13O} \qquad (3)$$

$$\theta_* = 1 - \theta_{C13O} - \theta_{C12O} \qquad (4)$$
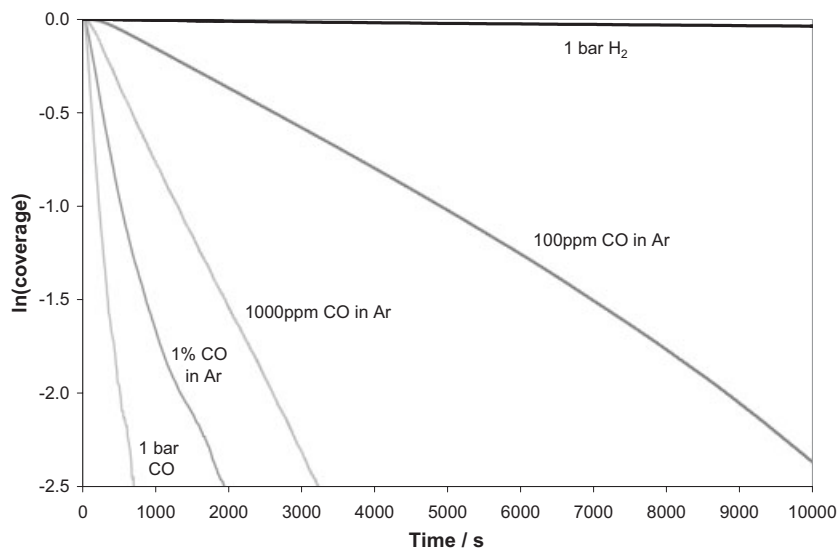
Fig. 6 Plot of ln of the normalised coverage versus time for a preadsorbed overlayer of $C^{13}O$ under flows of various gases and gas mixtures.

For a simple model it is necessary to assume that the pressure of $C^{13}O$ above the surface is zero, although 1% of the gas adsorbing will in fact be $C^{13}O$ from the natural abundance of C^{13}. It is also assumed that, over the flow rate range used for these experiments (12–15 ml min), there is no readsorption of desorbed $C^{13}O$.
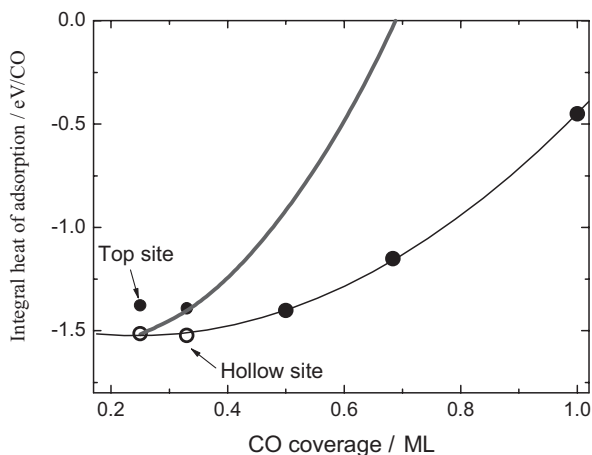

Fig. 7 The integral heats of adsorption for CO on Pt(111) at different coverages calculated using DFT. The lower thin line is the second order polynomial fit to the most stable adsorption configuration whilst the upper thick line gives the differential heat of adsorption.
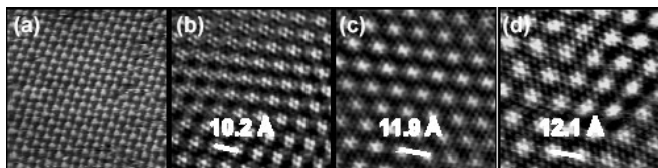

Fig. 8 STM images (75 × 75 Å2) of CO adsorption structures on Pt(111) at different CO pressures. (a) 1.33×10^{-7} mbar, (b) 1.33×10^{-2} mbar, (c) 133 mbar, (d) 960 mbar. Notice the change in the periodicity of the Moiré superstructure on (b)–(d).

Hence Eq. (3) reduces to:

$$\frac{d\theta_{C^{13}O}}{dt} = -k_1^- \theta_{C^{13}O} \qquad (5)$$

resulting in:

$$\theta_{C^{13}O} = \theta^o_{C^{13}O} e^{-k_1^- \cdot t} \qquad (6)$$

Thus the gradient of a plot of $\ln(\theta)$ *vs. t*, as observed in Figure 6, is a direct measurement of the rate of exchange.

The change in the rate of desorption for different partial pressures of CO (cf. Figure 6) necessarily derives from a change in the bonding energy of the CO. From these calculations on Pt(111) it is believed that a sharp decrease in the differential heat of adsorption of CO occurs for coverage above 0.5 ML (see Figure 7). Increasing the partial pressure of CO above the surface leads to a subsequent increase in coverage and the strongly repulsive lateral interactions that result lead to a significant increase in the rate of desorption.

In addition, the pressure dependence of the CO saturation coverage on Pt(111) was directly observed by in situ high pressure (HP) scanning tunnelling microscopy (STM). The combination of the home-built Aarhus [42] UHV STM with a novel HP STM (described in detail elsewhere [37]) facilitated *in situ* scanning on Pt(111) in a CO atmosphere over 13 orders of magnitude of pressure, ranging from 10^{-10} mbar up to 1 bar.

The CO adsorption structure was characterized at varying CO pressures. At 10^{-10} mbar and at temperatures slightly below room temperature (–28 °C) the c(4 × 2) commensurate overlayer was found (Figure 8a) [43], that can also be observed by LEED on room temperature samples [28]. Increasing the CO pressure to $> 6.7 \times 10^{-5}$ mbar results in the formation of a new CO adsorption structure (Figure 8b–d), in which a hexagonal superstructure with a periodicity of 3–4.5 times the periodicity of the substrate platinum is observed. Such a hexagonal superstructure has previously been found at 1 bar of CO on Pt(111) [32] in the form of a so-called Moiré structure. Such a superstructure arises from the interference between the hexagonally packed Pt surface and the hexagonally packed CO overlayer, which is rotated with respect to the Pt. Further details will be published elsewhere [44].

The reversibility of the formation of these CO Moiré structures was investigated by performing experiments where a given CO pressure was reached following different routes, either by lowering the pressure from a higher value or by increasing the pressure from a lower value. In both types of experiments the same CO adsorption structure was found. This implies that the Moiré structure changes reversibly and continuously with CO pressure. The latter is illustrated in Figure 9, in which the periodicity of the Moiré superstructure relative to the platinum substrate has been plotted for differ-
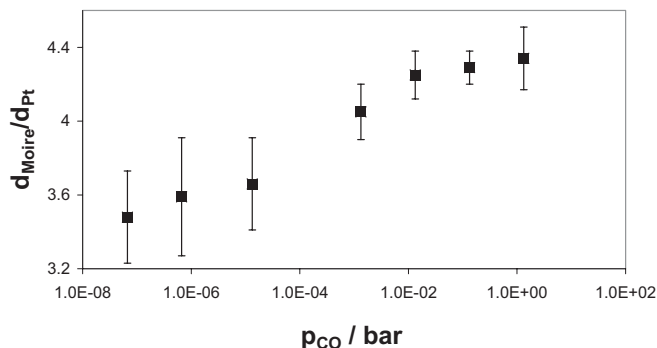
Fig. 9 The periodicity of the Moiré superstructure as a function of the CO pressure. $d_{Moiré}$ is the distance between adjacent Moiré patterns and d_{Pt} is the nearest-neighbour distance of the atoms on the Pt(111) surface.
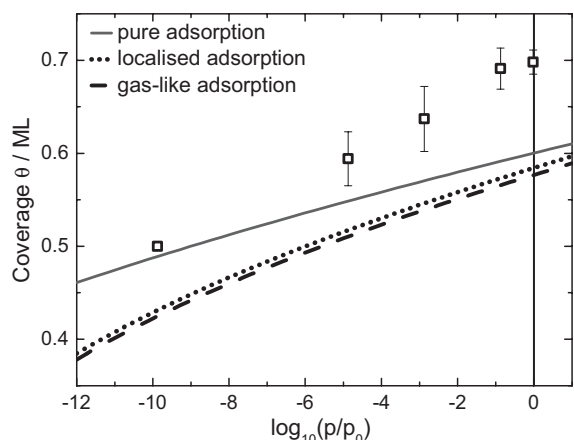

Fig. 10 The experimental data shows the CO coverage versus the CO pressure as measured with the HP STM. Also shown is the calculated equilibrium coverage of CO on the Pt(111) surface at room temperature (see text). The solid line represents the adsorption model not including any effects related to the statistics of CO adsorption on the surface. The dotted line is for the lattice gas model, and the dashed line represents a model of the mobile CO at the surface.

ent CO pressures. From high resolution STM images, such as those in Figure 8, the CO distance can be directly extracted by counting the individual CO molecules, and in this way the CO coverage can be determined as a function of the CO pressure. This has been plotted in Figure 10, where a clear pressure dependence of the CO coverage is observed.

5 Model of Adsorption

Calculated adsorption properties of CO provide a good starting point for the construction of a simple model of adsorption kinetics, which will be further used to compare with the experimental data presented above.

The equilibrium chemical potential of CO in the gas phase must be equal to that of the adsorbed state ($\mu_{gas} = \mu_{ads}$). From microscopic theory the chemical potential of an ideal gas $\mu_{gas} = -k_B T \frac{\partial \ln(Q_g)}{\partial N_g}$ is given by:

$$\mu_{gas} = -k_B T \ln\left(\frac{(2\pi M k_B T)^{3/2}}{h^3} \frac{k_B T}{p_0}\right) + \mu_{vib-rot} + k_B T \ln\left(\frac{p}{p_0}\right)$$

$$= -TS_0 + k_B T \ln\left(\frac{p}{p_0}\right) \tag{7}$$

where Q_g is the partition function for the ideal CO gas and $M = (m_O + m_C)$ is the mass of the gas molecule, h is Planck's constant, $\mu_{vib-rot}$ are the contribution from the vibrational and rotational degrees of freedom, and p and p_0 are the actual and standard pressures, respectively. The entropic term can be calculated from the microscopic model. The lengthy formulas for rotational and vibrational modes can be found in good textbooks [45]. Also, S_0 can be found in standard thermodynamic tables [46] and for CO $S_0 = 197$ J kmol^{-1} at standard thermodynamic conditions.

The chemical potential of adsorbed CO depends on the specific model used to describe adsorption. Two extreme cases are usually considered: localized adsorption, where adsorbed molecules are fixed at the adsorption sites (thus do not move on the surface) and mobile adsorption, where the adsorbent is free to move on the surface. It is safe to assume that the properties of CO are somewhere between these extremes. The chemical potential of adsorbed CO consists of contributions from the particular lattice statistics (μ_{stat}), vibrational properties ($\mu_{frus-vib}$) and both surface and mutual CO interaction (μ_{int}).

$$\mu_{ads} = \mu_{int} + \mu_{stat} + \mu_{frus-vib} \tag{8}$$

To determine the chemical potential of adsorbed CO the coverage $\theta = \frac{N}{M} = \frac{N_a}{A}$ is introduced where N molecules are adsorbed on M available sites, or they cover an area N_a of the total surface area available, A. The interaction part of the free energy can be determined directly from the DFT calculations, as the coverage dependence of $E_{ads}(\theta)$ is known (see Figure 7). Hence:

$$\begin{aligned}
\mu_{int} &= -k_B T \frac{\partial \ln\left((q_{ads})^N\right)}{\partial N} \\
&= -k_B T \frac{\partial \ln \exp(-N E_{ads}^{int}(\theta)/k_B T)}{\partial N} \\
&= k_B T \frac{\partial N E_{ads}^{int}(\theta)/k_B T}{\partial N} = \left(E_{ads}^{int}(\theta) + \theta \frac{\partial E_{ads}^{int}(\theta)}{\partial \theta}\right) = E_{ads}^{diff}
\end{aligned} \tag{9}$$

which is simply the differential heat of adsorption. This treatment of the interaction is purely phenomenological, as the details of the interaction energy are not considered, which is an obvious limitation, but there is a great advantage to this approach, which is that the model can be solved analytically.

In the case of localised adsorption, all gas translational and rotational degrees of freedom are lost in favour of frustrated vibrational modes of the adsorbed CO molecule. This part of the chemical potential can be written as:

$\mu_{frus-vib} = -k_B T \ln(q_{frus-vib})$, where the vibrational partition function runs over all modes:

$$q_{frus-vib} = \sum_i \exp(-\varepsilon_i/2k_B T)/[1 - \exp(h\omega_i/k_B T)].$$

Finally the statistics of the adsorbed phase give the configurational entropy for the localised adsorption:

$$\mu_{stat} = -k_B T \partial \ln\left(\frac{M}{(M-N)N}\right)/\partial N = -k_B T \ln\left(\frac{\theta}{1-\theta}\right).$$

Notice that this is a standard expression for lattice models, but it is also valid for mobile adsorption, as long as the finite size of CO is taken into account. In the limit of point molecules the formula reduces to that of a 2-dimensional ideal gas. If CO is mobile at the surface, a very reasonable assumption as there is only a very small difference between the CO adsorption energies at different surface sites, then this has to be taken into account, and an additional term enters the free energy, equivalent to the pressure in a 3-dimensional gas and equal to $k_B T \frac{\theta}{1-\theta}$.

The chemical potential of adsorbed CO equals:

$$\mu_{ads} = E_{ads}^{int}(\theta) + \theta \frac{\partial E_{ads}^{int}(\theta)}{\partial \theta} + \mu_{stat} + \mu_{frus-vib} \qquad (10)$$

and the last term varies with the adsorbent properties. $\mu_{stat} = k_B T \ln\left(\frac{\theta}{(1-\theta)}\right)$ for localised adsorption and

$$\mu_{stat} = k_B T \ln\left(\frac{\theta}{(1-\theta)}\right) + k_B T \left(\frac{\theta}{(1-\theta)}\right) \text{ for mobile adsorption.}$$

In the latter case $\mu_{frus-vib}$ will be the normal $\mu_{vib-rot}$.

To find the equilibrium CO coverage the differential heat of adsorption needs to be calculated, which can be done easily by approximating discrete points from DFT by a simple continuous function. The approximation by the second order polynomial is shown on Figure 7, and it is used in further considerations. The equilibrium temperature of the diluent gas (argon) and the surface ensures that effects related to direct energy transfer between impinging molecules and adsorbed CO is of minor importance.

The calculated equilibrium CO coverage on the Pt(111) surface at various pressures is shown with the experimental data in Figure 10. The three lines represent three different models for the adsorbent. Note that there is a very small difference between the two extreme adsorption statistics, and an almost linear regime in all interesting pressure ranges. The precise determination of CO coverage is beyond the scope of the present paper, but comparing to existing literature fairly good agreement is found. From the STM data presented in this paper and in Ref. [32] a room temperature coverage of 0.68 ML at ambient pressure, and around 0.5 ML in UHV, are observed. A simplistic mean field model as presented above is not able to predict the formation of superstructures, such as the c(4 × 2) structure observed for CO on Pt(111). This is one of the reasons why the calculated equilibrium CO coverage is lower than the experimental.

Determination of the desorption rate, k, is now very simple, as the desorption mechanism is governed simply by Eq. (6). The standard desorption rate at equilibrium is given by: $k_1^- = \nu(\theta) \exp\left(-\frac{E_{act}(\theta)}{k_B T}\right)$, where $\nu(\theta)$ is the prefactor, and $E_{act}(\theta)$ is the activation energy.

If CO adsorption is not activated then $E_{act} = E_{ads}^{diff}$.

For CO on Pt(111), however, Steckel et al. [47] have shown that at a coverage above 0.6 ML a barrier for desorption appears. While it is very small, 0.1 eV for 0.6 ML, the magnitude of this barrier grows to 0.5 eV at 1 ML. One might argue, that such a high coverage is not possible for such a system as CO on Pt(111), but the existence of a barrier, however small, at a coverage around 0.6 ML influences the desorption process. The activation barrier is given by $E_{act} = -E_{ads}^{diff} + \xi E_{ads}^{diff}$, and $0 < \xi < 1$ is a continuous function of the coverage.

By assuming that there is a chemical equilibrium between the adsorbed CO and the CO in the gas phase Eq. (7) and (10) can be equated, i.e.:

$$\mu_g = \mu_{ads}$$

$$\Rightarrow \ln\left(\frac{p}{p_0}\right) - \frac{S_0}{k_B} = \frac{E_{ads}^{int}(\theta)}{k_B T} + \frac{\theta}{k_B T}\frac{\partial E_{ads}^{int}(\theta)}{\partial \theta} + \frac{\mu_{stat}}{k_B T} + \frac{\mu_{frus-vib}}{k_B T}$$

$$\Rightarrow \frac{E_{ads}^{diff}(\theta)}{k_B T} = \ln\left(\frac{p}{p_0}\right) + \frac{\mu_{rest}}{k_B T}$$

where all the terms with small coverage dependence have been collected in the term μ_{rest}. Now, utilising the fact that the activation energy can be expressed in terms of the adsorption energy and that $\ln(k_1^-) = \ln(\nu(\theta)) - \frac{E_{act}(\theta)}{k_B T}$ then:

$$\ln(k_1^-) = \ln(\nu(\theta)) - \frac{E_{act}(\theta)}{k_B T}$$

$$= \ln(\nu(\theta)) + (1-n)\ln\left(\frac{p}{p_0}\right) + (1-n)\frac{\mu_{rest}}{k_B T}$$

$$= (1-n)\ln\left(\frac{p}{p_0}\right) + \alpha$$

A relationship between the pressure and the rate constant is arrived at, where coefficients (1-n) and α come from Figure 10. The slope of the linear relation depends on the coverage dependence of the activation energy, which is usually taken as minus the adsorption energy.

This means that the coverage dependence of the activation energy is weaker than the adsorption energy. The relation between p and k is presented in Figure 11. The absolute location along the k axis is determined by the prefactor, ν, and a value of $\nu = 10^{17}$ gives good agreement with the experimental data.

It is then possible to convert the rates observed for CO desorption to equivalent current densities that would be required to oxidise the same amount of CO. The case at 1 bar of CO was considered where an average desorption rate of 6.52×10^{-3} s^{-1} was obtained.
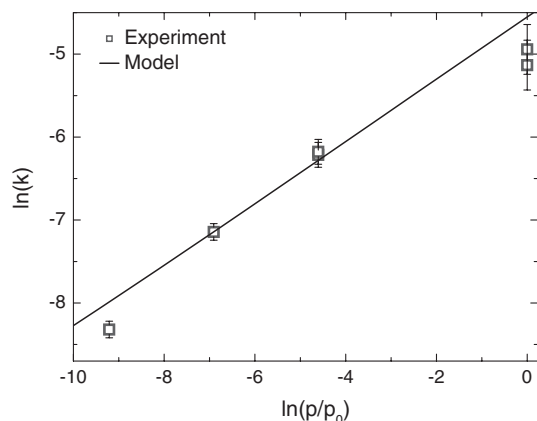
Fig. 11 Plot of the rate of $C^{13}O$ desorption versus the pressure of $C^{12}O$ above the surface. Squares represent experimental data whilst the solid line is from the simple model described in the text.

If a prefactor of 10^{17} is assumed, an activation energy can be found from the expression:

$$k_{des} = ve^{\frac{-E_{des}(\theta)}{k_b T}} \tag{10}$$

A value of 1.13 eV is obtained.

By substituting back into Eq. 10, extrapolated values for the rate of desorption of CO at 62 °C and 80 °C can be obtained. As the number of sites per square centimetre is 1.50×10^{15} for close-packed Pt(111) and the number of electrons per oxidised CO molecule is 2, then these rates can be converted to equivalent oxidation currents:

At 25 °C $k = 6.5 \times 10^{-3}$ s^{-1}; $j = 3.1 \times 10^{-3}$ mA cm^{-2}

At 62 °C $k = 0.85$ s^{-1}; $j = 0.41$ mA cm^{-2}

At 80 °C $k = 6.3$ s^{-1}; $j = 3.0$ mA cm^{-2}

Using a value for the prefactor of 10^{13} s^{-1} the value of the desorption energy reduces to 0.90 eV and the following values for k and j are obtained:

At 25 °C $k = 6.5 \times 10^{-3}$ s^{-1};
             $j = 3.1 \times 10^{-3}$ mA cm^{-2}

At 62 °C $k = 0.31$ s^{-1};
             $j = 0.14$ mA cm^{-2}

At 80 °C $k = 1.5$ s^{-1};
             $j = 0.73$ mA cm^{-2}

To determine the effect this would have on the fuel cell anode mechanism, it is necessary to compare these rates with values directly measured for the CO oxidation
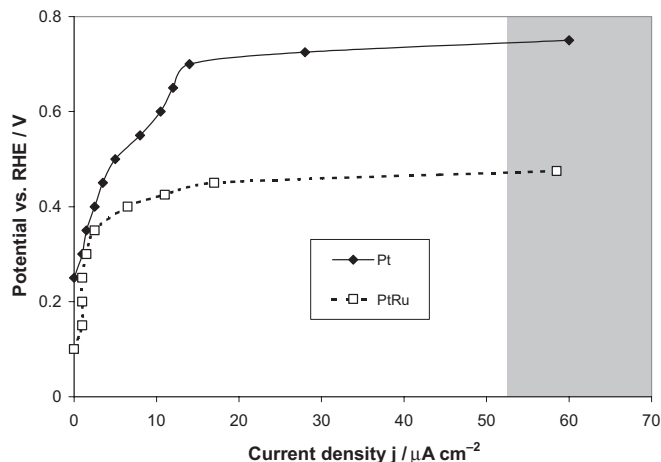

Fig. 12 Experimentally observed polarisation curve for CO (100%) oxidation at 62 °C on a platinum/ruthenium surface alloy electrode with the relative surface ratio of 50:50, reproduced from Ref. [12]. The shaded region shows the calculated range of equivalent current densities obtained from the experimental CO desorption rate for 100% CO, on varying the prefactor from 10^{13} to 10^{17}, and extrapolated to 62 °C.

rates at the given temperatures as governed by the relationship shown earlier in Eq. (1). Figure 12 shows the potential required to provide a current density, j, for the oxidation of pure CO at 25 °C calculated from experimental data [12]. If it can be shown that the equivalent current densities calculated above would require significant overpotentials, which are not observed as potential losses for the fuel cells operating at these temperatures then the desorption rate must be significant compared to the oxidation rate under the operating conditions of the fuel cell.
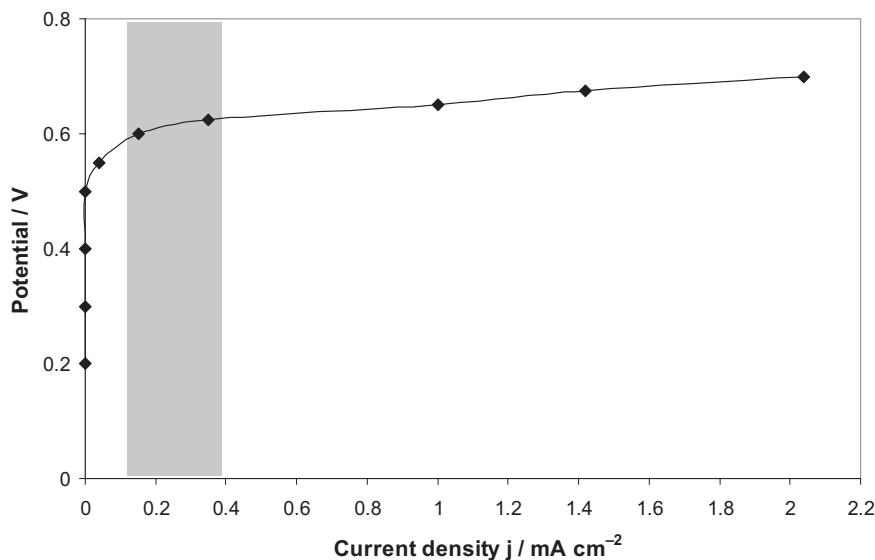

Fig. 13 Experimentally observed polarisation curve for CO (2% in argon) oxidation at 62 °C on a platinum/ruthenium surface alloy electrode with the relative surface ratio of 50:50 (reproduced from Ref. [12]). The shaded region shows the calculated range of equivalent current densities obtained from the experimental CO desorption rate for 1% CO in argon, on varying the prefactor from 10^{13}–10^{17}, and extrapolated to 62 °C. The upper limit is 150 µA cm^{-2} and is not shown on this plot.

If the data for the rate of CO desorption on pure Pt, and the rate of oxidation of pure CO on a platinum/ruthenium 50:50 surface alloy are compared, then it can be seen that, for the oxidation rate to match the desorption rate (j = 0.12 mA cm^{-2}) then an overpotential of ~0.6 V would be required. On pure platinum this value would be even higher.

If a similar treatment for the data at 1% CO in Ar is conducted for a prefactor of 10^{17} and at a temperature of 62 °C, a current density of j = 0.15 mA cm^{-2} is observed whereas for a prefactor of 10^{13}, j = 0.053 mA cm^{-2}. This gives a possible range for the current density obtained.

Again comparing to the data of Gasteiger et al. [12] in Figure 13, obtained for the pure oxidation of 2% CO in argon at 62 °C and comparing directly to our figure of between 53–150 μA cm^{-2} it can be seen that an overpotential of at least 0.7 V would be required on pure platinum and an overpotential of 0.45 V required on PtRu to provide the same rate of removal of CO by oxidation.

Therefore this would suggest that the rate of desorption is indeed significant in comparison to the rate of oxidation observed in the fuel cell gas stream. That is to say, that at overpotentials below those designated by the grey areas in Figures 12 and 13, the rate of desorption of CO will exceed the rate of electrochemical oxidation and the surface coverage would be determined by the thermal equilibrium coverage. The only reservation can be, whether the presence of water in the gas stream significantly reduces the CO desorption rate, and this is the subject of an ongoing study. It seems likely, however, that the dry gas phase behaviour will be a closer model to the behaviour in the humidified fuel cell set-up than that observed in solution where some limitation on the exchange rate is likely.

6 Conclusions

It has been shown from CO isotope exchange experiments that there is a significant CO exchange rate on platinum fuel cell catalysts at room temperature. Moreover, this rate of desorption is strongly dependent on the pressure of CO in the feed gas to the fuel cell.

DFT calculations have demonstrated that increasing the pressure of CO above the platinum surface leads to an increase in the coverage of CO on the surface and a concomitant drop in the binding energy for CO. The coverage dependency on pressure has been demonstrated using a high pressure STM from the range of ultra-high vacuum up to 1 bar.

Furthermore, it has been demonstrated that adsorbed CO is not caused to desorb by a stream of hydrogen at room temperature.

It is believed that in a fuel cell running under normal conditions at 80 °C the partial pressure of CO in the feed gas will strongly affect the CO coverage, binding energy and subsequent desorption rate, and that these factors are all intricately linked in the mechanism leading to the improved tolerance of the fuel cell.

Furthermore, it has been demonstrated that the rate of desorption is indeed significant compared to the rate of oxidation observed in a fuel cell.

References

[1] G. Hoogers, D. Thompsett, *CATTECH* **1999**, *3*, 106.

[2] R. A. Lemons, *J. Power Sources* **1990**, *29*, 251.

[3] W. Vogel, J. Lundquist, P. Ross, P. Stonehart, *Electrochim. Acta* **1975**, *20*, 79.

[4] H. Igarashi, T. Fujino, M. Watanabe, *J. Electroanal. Chem.* **1995**, *391*, 119.

[5] H. F. Oetjen, V. M. Schmidt, U. Stimming, F. Trila, *J. Electrochem. Soc.* **1996**, *143*, 3838.

[6] M. Watanabe, S. Motoo, *J. Electroanal. Chem.* **1975**, *60*, 267.

[7] S. Motoo, M. Watanabe, *J. Electroanal. Chem.* **1979**, *98*, 203.

[8] H. A. Gasteiger, N. Markovic, P. N. Ross, E. J. Cairns, *J. Phys. Chem.* **1994**, *98*, 617.

[9] H. A. Gasteiger, P. N. Ross, E. J. Cairns, *Surf. Sci.* **1993**, *293*, 67.

[10] H. A. Gasteiger, N. Markovic, P. N. Ross, E. J. Cairns, *Electrochimica Acta* **1994**, *39*, 1825.

[11] H. A. Gasteiger, N. Markovic, P. N. Ross, *J. Phys. Chem.* **1995**, *99*, 8290.

[12] H. A. Gasteiger, N. Markovic, P. N. Ross, *J.Phys. Chem.* **1995**, *99*, 16757.

[13] J. C. Davies, B. E. Hayden, D. J. Pegg, *Electrochimica Acta* **1998**, *44*, 1181.

[14] J. C. Davies, B. E. Hayden, D. J. Pegg, *Surf. Sci.* **2000**, *467*, 118.

[15] J. C. Davies, B. E. Hayden, M. E. Rendall, D. J. Pegg, *Surf. Sci.* **2002**, *496*, 110.

[16] M. T. M. Koper, T. E. Shubina, R. A. van Santen, *J. Phys. Chem. B* **2002**, *106*, 686.

[17] T. E. Shubina, M. T. M. Koper, *Electrochimica Acta* **2002**, *47*, 3621.

[18] P. Liu, A. Logadottir, J. K. Norskov, *Electrochimica Acta* **2003**, *48*, 3731.

[19] H. Igarashi, T. Fujino, Y. M. Zhu, H. Uchida, M. Watanabe, *Phys. Chem. Chem. Phys.* **2001**, *3*, 306.

[20] M. Watanabe, Y. M. Zhu, H. Igarashi, H. Uchida, *Electrochemistry* **2000**, *68*, 244.

[21] P. Wolohan, P. C. H. Mitchell, D. Thompsett, S. J. Cooper, *J. Mol. Catal. A* **1997**, *119*, 223.

[22] R. J. Behm, *Acta Physica Polonica A.* **1998**, *93*, 259.

[23] Q. Ge, S. Desai, M. Neurock, K. Kourtakis, *J. Phys. Chem. B.* **2001**, *105*, 9533.

[24] M.-S. Liao, C. R. Cabrera, Y. Ishikawa, *Surf. Sci.* **2000**, *445*, 267.

[25] Y. Ishikawa, M.-S. Liao, C. R. Cabrera, *Surf. Sci.* **2002**, *513*, 98–110.

[26] E. Christoffersen, P. Liu, A. Ruban, H. L. Skriver, J. K. Norskov, *J. Catal.* **2001**, *199*, 123.

[27] M. Watanabe, M. Shibata, S. Motoo, *J. Electroanal. Chem.* **1986**, *206*, 197.

[28] G. Ertl, M. Neumann, K. M.Streit, *Surf. Sci.* **1977**, *64*, 393.

[29] W. D. Mieher, L. J. Whitman, W. Ho, *J. Chem. Phys.* **1989**, *91*, 3228.

[30] H. Steininger, S. Lehwald, H. Ibach, *Surf. Sci.* **1982**, *123*, 264.

[31] B. E. Hayden, A. M. Bradshaw, *Surf. Sci.* **1983**, *125*, 787.

[32] E. K. Vestergaard, P. Thostrup, T. An, E. Lægsgaard, I. Stensgaard, B. Hammer, F. Besenbacher, *Phys. Rev. Lett.* **2002**, *88*, 259601.

[33] Y. Y. Yeo, L. Vattuone, D. A. King, *J. Chem. Phys.* **1997**, *106*, 392.

[34] T. Matsushima, *Surf. Sci.* **1979**, *79*, 63.

[35] D. H. Parker, A. D. Fisher, J. Colbert, B. E. Koel, J. L. Gland, *Surf. Sci.* **1991**, *258*, 75.

[36] B. Kasemo, *Rev. Sci. Instrum.* **1979**, *50*, 1602.

[37] E. Lægsgaard, L. Österlund, P. Thostrup, P. B. Rasmussen, I. Stensgaard, F. Besenbacher, *Rev. Sci. Instrum.* **2001**, *72*, 3537.

[38] B. Hammer, L. B. Hansen, J. K. Nørskov, *Phys. Rev. B.* **1999**, *59*, 7413.

[39] D. Vanderbilt, *Phys. Rev. B.* **1990**, *41*, 7892.

[40] G. Kresse, J. Furthmuller, *Comput. Mat. Sci.* **1996**, *6*, 15.

[41] M. Mavrikakis, B. Hammer, J. K. Nørskov, *Phys. Rev. Lett.* **1998**, *81*, 2819.

[42] F. Besenbacher, *Reports on Progress in Physics* **1996**, *59*, 1737.

[43] M. Ø. Pedersen, M.-L. Bocquet, P. Sautet, et al., *Chemical Physics Letters* **1999**, *299*, 403.

[44] E. K. Vestergaard, R. T. Vang, J. Schnadt, S. Longwitz, F. Besenbacher, in preparation.

[45] T. L. Hill, *An Introduction to Statistical Thermodynamics*, Addison-Wesley, Reading, USA, **1960**.

[46] *CRC Handbook of Chemistry and Physics*, 64th ed. (Eds. R. C. Weast), CRC, Boca Raton, FL, **1985**.

[47] J. A. Steckel, A. Eichler, J. Hafner, *Phys. Rev. B.* **2003**, *68*, 85416.

_____